Obrabotka metallov (tekhnologiya, oborudovanie, instrumenty) = Metal Working and Material Science. 2025 vol. 27 no. 2 pp. 142–158
ISSN: 1994-6309 (print) / 2541-819X (online)
DOI: 10.17212/1994-6309-2025-27.2-142-158

NSTU NETI

Obrabotka metallov - Metal Working and Material Science

Journal homepage: http://journals.nstu.ru/obrabotka_metallov

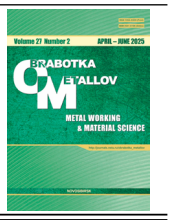

Manufacturing conditions of bimetallic samples based on iron and copper alloys by wire-feed electron beam additive manufacturing

Ksenia Osipovich [a, *], ***Evgeny Sidorov*** [b], ***Andrey Chumaevskii*** [c], ***Sergey Nikonov*** [d], ***Evgeny Kolubaev*** [e]

Institute of Strength Physics and Materials Sciences SB RAS, 2/4, pr. Akademicheskii, Tomsk, 634055, Russian Federation

[a] https://orcid.org/0000-0001-9534-775X, osipovich_k@ispms.ru; [b] https://orcid.org/0009-0009-2665-7514, eas@ispms.ru;
[c] https://orcid.org/0000-0002-1983-4385, tch7av@gmail.com; [d] https://orcid.org/0000-0002-5588-4718, SergRFF@ispms.ru;
[e] https://orcid.org/0000-0001-7288-3656, eak@ispms.tsc.ru

ARTICLE INFO

Article history:
Received: 09 April 2025
Revised: 17 April 2025
Accepted: 21 April 2025
Available online: 15 June 2025

Keywords:
Additive manufacturing
Wire-feed electron beam additive manufacturing (*EBAM*)
Sharp interface
Smooth interface
Heterogeneous structure
Heat input
Macrostructure

Funding
The investigation was supported by the Russian Science Foundation grant No. 24-72-00118.

ABSTRACT

Introduction. Wire-feed electron beam additive manufacturing (*EBAM*) is a promising production technology, offering unprecedented control over interface design in composite materials, which is challenging to achieve using conventional methods. The ability to control localized metallurgical processes within the melt pool is a key advantage of *EBAM* technology. This study investigates the influence of key *EBAM* parameters (wire feed configuration, scanning strategies, and linear energy input) on achieving diverse interface designs in bimetallic samples composed of copper and iron-based alloys. Establishing the relationship between microstructure evolution and 3D printing parameters is of great importance for the development of *EBAM*. **The purpose of this study** is to elucidate the effects of fundamental *EBAM* process parameters (beam current, wire feed rate, heat input, scanning strategy, and intrinsic material properties) on the fabrication of high-quality copper-iron bimetallic samples exhibiting both sharp and smooth interfaces, as well as heterogeneous material distributions. **Research Methods.** This study heavily emphasizes experimental investigations to optimize the *EBAM* process. Bimetallic samples featuring sharp interfaces, smooth interfaces, and heterogeneous microstructures, based on copper and iron alloys, were fabricated using wire-feed *EBAM*. The study analyzed the values of heat input depending on the layer being deposited; the wire feed rate depending on the material used, and the types of printing strategies depending on the ratio of dissimilar materials in bimetallic samples. A *Pentax K-3* digital camera, equipped with a 100 mm focal length lens, was employed for high-resolution visual inspection and quality assessment of the fabricated bimetallic samples with varying interface designs. **Results and discussion.** Based on an in-depth understanding of the factors governing electron beam-material interactions, this work systematically details the potential for creating components with controlled sharp or smooth interfaces, as well as heterogeneous material architectures. Furthermore, the study briefly outlines process control methodologies aimed at minimizing defects, considering factors influencing melt pool dynamics, including the precise regulation of thermal conditions during 3D printing process. A fixed heat input was prescribed for each material to achieve a sharp interface morphology: specifically, 0.09 kJ/mm for the deposition of *M1* copper layers, which is 2.5 times lower than the heat input used for depositing *Cu-9 Al-2 Mn* copper alloy layers. Similarly, a heat input of 0.17 kJ/mm was used for *0.12 C-18 Cr-9 Ni-Ti* stainless steel layers, which is 1.5 times lower than that for *0.09 C-2 Mn-Si* steel alloy layers. In contrast, the fabrication of smooth interfaces relied on dynamically adjusting the heat input and wire feed rates as a function of the layer being deposited and the target composition. The formation of heterogeneous structures required the use of tailored scanning strategies during *EBAM*, depending on the volume fraction of dissimilar alloys deposited via the wire feedstock. The successful fabrication of defect-free copper-iron bimetallic samples was achieved through careful control of the *EBAM* process.

For citation: Osipovich K.O., Sidorov E.A., Chumaevskii A.V., Nikonov S.N., Kolubaev E.A. Manufacturing conditions of bimetallic samples based on iron and copper alloys by wire-feed electron beam additive manufacturing. *Obrabotka metallov (tekhnologiya, oborudovanie, instrumenty) = Metal Working and Material Science*, 2025, vol. 27, no. 2, pp. 142–158. DOI: 10.17212/1994-6309-2025-27.2-142-158. (In Russian).

Introduction

Modern additive manufacturing methods, such as wire electron beam 3D printing (*EBAM*), represent one of the most promising approaches to creating complex metallic structures with unique mechanical and functional properties. Currently, the number of publications on the fabrication of bimetallic specimens using electron beam methods is growing, confirming the relevance of this research. This method is actively used in aerospace, automotive, and medical industries, where high precision, strength, and reliability of products

*** Corresponding author**
Osipovich Kseniya S., Ph.D. (Physics and Mathematics)
Institute of Strength Physics and Materials Sciences SB RAS,
2/4, pr. Akademicheskii,
634055, Tomsk, Russian Federation
Tel.: +7 999 499-57-53, **e-mail:** osipovich_k@ispms.ru

are required [1]. Unlike traditional casting and milling methods, *EBAM* allows fabricating products from dissimilar materials with minimal material loss and without the need for molds and dies [2].

A bimetallic specimen is manufactured from two materials with different properties, which makes it possible to obtain a product with property characteristics distinct from those of the individual materials used. Bimetals should not have defects at the interface between dissimilar materials. When defects occur, specimens lose the required parameters of mechanical or operational properties. The most common design of the interface in bimetallic specimens is an abrupt transition from one material to another. The most common example of such materials is bimetals with a sharp interface based on the "steel-copper" system, manufactured using laser sintering [3, 4]. However, analysis of the literature has shown that creating a smooth interface between dissimilar materials when using the laser sintering method is difficult. Therefore, *EBAM* provides unprecedented freedom of microstructural design during manufacturing.

One of the fundamental aspects affecting *EBAM* efficiency is the interaction of the electron beam with the metal wire [5]. The theory of electron scattering plays an important role in determining the depth of beam penetration, the shape and size of the melt pool, as well as in controlling the heat flows that affect material crystallization [6]. Insufficient attention to these factors can lead to reduced mechanical strength, deteriorated geometric accuracy, and an increased number of defects in finished products [7]. Understanding these processes allows predicting microstructure formation, minimizing defects such as porosity, cracks, and structural heterogeneity, as well as optimizing printing parameters to achieve the best results [8]. The process is based on a cathode assembly, which increases energy to overcome the potential barrier due to high temperature and the potential difference between anode and cathode [9]. In addition to the cathode assembly, electron guns operate to form and focus directed electron beams, which are accelerated under the action of an electric field and focused by a magnetic field, forming a directed electron beam [10]. The focused electron beam emitted by the cathode, under the influence of high temperatures, converts the released thermal energy, thereby forming local heating and melting the material. Through the simultaneous operation of the wire feeder and the electron beam along a predetermined trajectory, the material is built up layer by layer, forming a three-dimensional structure after solidification. Depending on the amount of energy emitted by the beam, the intensity of scattering will be greater at a lower energy value. However, at a higher energy value, there is a probability of expanding the heat-affected zone, which leads to excessive penetration of the fed wire onto the substrate or already deposited layers. The scanning size in electron beam 3D printing is directly related to the diameter of the electron beam and its interaction with the material. Increasing electron energy leads to greater penetration depth, but also expands the scattering area, which can reduce the geometric accuracy of the manufactured product [1]. To minimize this effect, it is necessary to optimize beam parameters such as energy, focus, and current density. For example, studies show that using an electron beam with low energy allows achieving higher geometric accuracy of the manufactured product, but limits the thickness of the applied layer [2]. At high electron beam energy and low scanning speed, energy will concentrate in the surface layers, which can lead to local overheating, and vice versa. At optimal parameters, energy is evenly distributed throughout the volume, ensuring stable melting and formation of high-quality macro- and microstructure. Insufficient energy transfer, due to electron scattering, can cause incomplete melting of the material, which contributes to the formation of porosity in the structure of the product. In addition, insufficient energy can prevent the material from reaching the melting temperature, which negatively affects the strength of interlayer bonds and increases surface roughness. Also, uneven cooling associated with non-uniform energy distribution contributes to the formation of local stress zones, which can promote the formation of microcracks. These effects emphasize the importance of controlling electron beam parameters and accounting for scattering processes to minimize defects and improve the quality of printed products [11].

This paper examines the influence of the main *EBAM* process characteristics (current, feed rate, heat input, printing strategy, and material properties), which are part of the electron scattering theory, on the quality of the obtained products. Special attention is paid to experimental studies that allow optimizing the printing process. ***The aim of this work*** is to establish the influence of the main *EBAM* process characteristics (current, feed rate, heat input, printing strategy, and material properties) on the quality of the obtained

products for the formation of high-quality bimetallic specimens with sharp and smooth interfaces, and heterogeneous structure based on copper and iron alloys. To achieve this aim, ***the following tasks*** were solved during the research:

– establishing the ranges of heat input values when applying layers based on iron and copper alloys for the formation of a sharp interface, which depend on the values of voltage and current required for the formation of the melt pool;

– determining the ratio of feed rates of wires into the melt pool for the formation of a smooth interface;

– studying the influence of the type of printing strategy depending on the percentage ratio of the volume of dissimilar alloys with simultaneous feeding of wires into the melt pool.

Research methodology

Bimetallic specimens with different interface designs and heterogeneous structures were obtained using a laboratory experimental installation for additive electron beam manufacturing of metal products at ISPMS SB RAS (Fig. 1). Iron and copper alloys were selected as dissimilar materials. For iron alloys, 1.0 mm diameter wires of stainless steel *AISI 321* and structural low-alloy steel *0.09 C-2 Mn-Si* were used, while for copper alloys, 1.2 mm diameter wires of technically pure copper *M1* and tin-free bronze *Cu-9 Al-2 Mn* (Table 1) were used. The selection of these alloys was based on their wide practical applications (shipbuilding, aircraft construction, mechanical engineering, etc.).

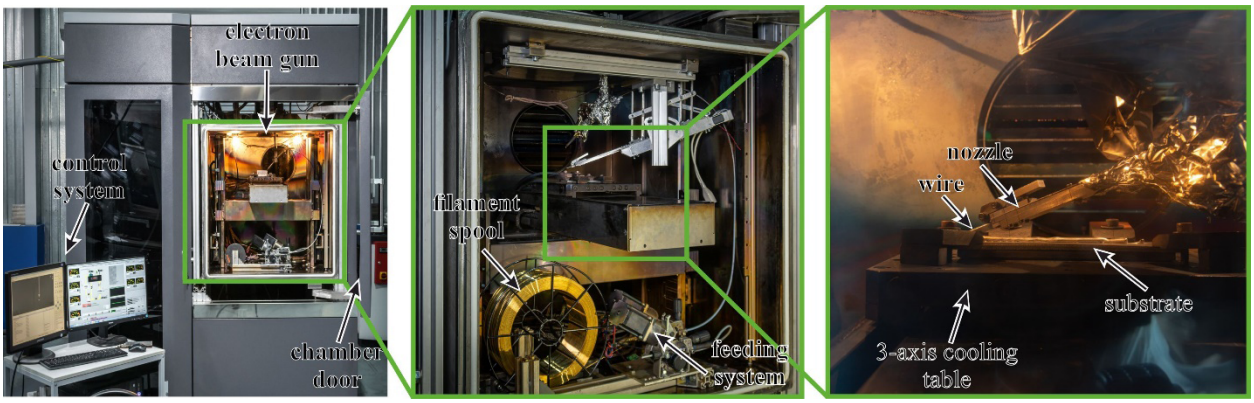

Fig. 1. Vacuum chamber of the laboratory experimental installation for electron beam additive manufacturing

Table 1

Chemical composition of wire feedstock: iron and copper alloys

Material		Chemical composition, wt.%								
		Fe	*Cu*	*Cr*	*Ni*	*Mn*	*Al*	*Si*	*C*	Other
Substrate	*AISI 304*	Bal.	≤ 0.3	17-19	9-11	≤ 2	–	≤ 0.8	≤ 0.08	to 1.1
Wire	*AISI 321*	Bal.	≤ 0.3	17-19	9-11	≤ 2	–	≤ 0.8	≤ 0.12	≤ 0.6
	M1	≤ 0.005	Bal.	–	to 0.002	–	–	–	–	≤ 0.02
	0.09 C-2 Mn-Si	Bal.	≤ 0.3	to 0.3	to 0.3	1.3-1.7	–	0.5-0.8	≤ 0.12	≤ 0.28
	Cu-9 Al-2 Mn	≤ 0.5	Bal.	–	–	1.5-2.5	8-10	to 0.1	–	≤ 1.65

Multi-component specimens were printed using an electron beam generated by an electron gun through a magnetic focusing system that forms a sweep on the surface in the printing area, forming a melt pool. The wire was fed from a feeder. As a result, a pattern consisting of layer-by-layer deposited material was formed on the substrate.

By varying the parameters during *EBAM*, this method is potentially suitable for producing materials with controlled structure and improved mechanical or performance characteristics. The printing parameters (sweep size, voltage, scanning frequency, current and wire feed rate) used to fabricate the vertical wall are summarized in Table 2.

Table 2

***EBAM* process parameters**

Material	Interface	Sweep shape	Sweep size, mm	Voltage U, kV	Scanning frequency, Hz	Current, mA	Deposition speed υ, mm/min
AISI 321-M1	Sharp / smooth / composite	Ellipse	5	30	1,000	90-45	250-440
AISI 321- Cu-9 Al-2 Mn						80-42	250-440
0.09 C-2 Mn-Si - Cu-9 Al-2 Mn						85-45	250-400

For visualization of the quality of grown bimetallic specimens with different designs, a *Pentax K-3* digital camera with a 100 mm focal length lens was used.

Results and discussion

A comprehensive understanding of the formation of specific structures and their design in the additive manufacturing process opens up extensive opportunities for obtaining bimetals with desired properties in specific parts of components, enabling the production of more efficient engineering products [12, 13]. Fig. 2 schematically shows some currently possible combinations for multi-material products in additive manufacturing. Depending on the product's purpose and requirements, various material deposition geometries and interface designs can be applied. As mentioned above, the simplest and most common interface design is sharp (Fig. 2, *a*). It is also possible to obtain a smooth interface between dissimilar materials (Fig. 2, *b*). Heterogeneous structures can also be obtained by simultaneously feeding dissimilar immiscible materials, using powder wire, or adding metal powder to the matrix material (Fig. 2, *c*). In particular, using inserts of a second material in the "matrix" of the first (separate areas of the product are printed by sequential deposition of the second material, while the remaining volume is printed with the first material). To create a more complex interface design, alternating dissimilar materials can be used, forming a layered structure (Fig. 2, *d*). The structure design can represent a periodic alternation of dissimilar bands (one through one, one through two, one through three... two through two, two through three, etc.). 3D printing of sequential layers with different materials is further relevant when creating volumetric products through the formation of adjacent (contiguous) columns or blocks. In practical applications, it may be desirable or even necessary to have three or more compositions, which is not difficult for additive manufacturing, which provides unprecedented freedom of structural design during fabrication.

To form a specific design of the structure of dissimilar materials, it is necessary to know the physical and mechanical properties of metals and alloys for additive manufacturing in order to unlock the full true potential and obtain a defect-free product [14]. For example, the manufacture of bimetallic specimens based on iron and copper alloys can provide unique material properties by combining the thermal conductivity and thermal expansion coefficient of copper with the high strength of steel (Table 3). However, the extremely

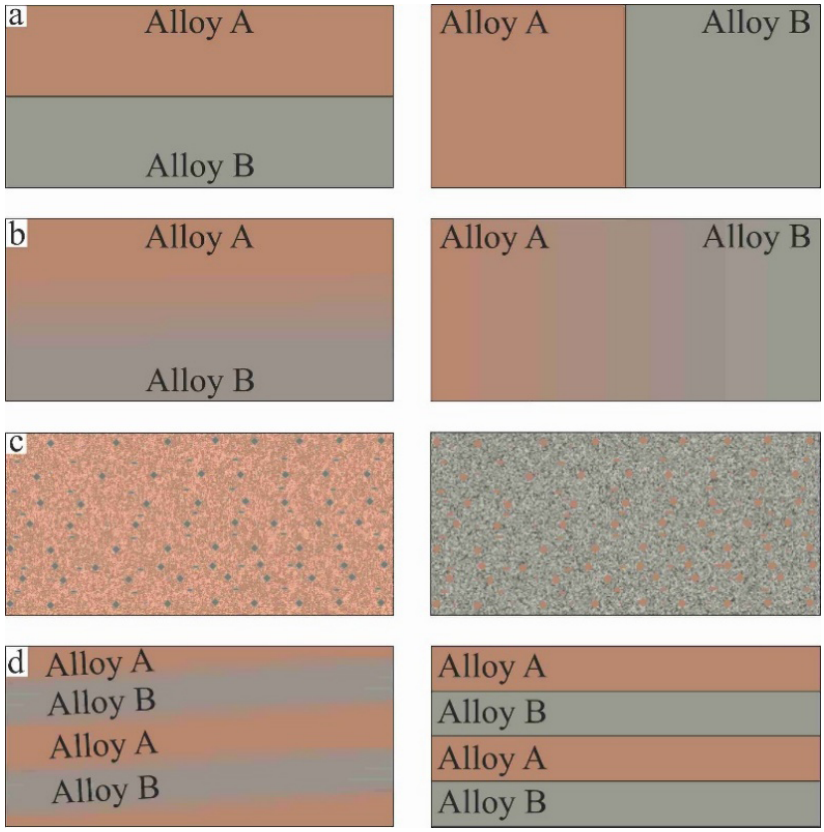

Fig. 2. Schematic of possible multi-component sample configurations fabricated by additive manufacturing:

a – sharp interface; *b* – smooth interface; *c* – heterogeneous structure; *d* – layered composite

Table 3

Physical and mechanical properties of the materials used

Material	T_m, °C	ρ, kg/m^3	*C*, J / (kg · °C)	λ, W / (m · °C)	α, 1 / °C
AISI 321	1,420	7,920	462-596	15-26	16.6-19.3
M1	1,083	8,940	390	387	16.7
0.09 C-2 Mn-Si	1,450-1,520	7,850	496-676	33-27	11.5-12.3
Cu-9 Al-2 Mn	1,060	7,630	461	71.4	17

low ability to absorb electron beam radiation (~2 %) and high thermal conductivity (400 W·m^{-1}·K^{-1}) of copper and copper alloys mean that high heat input values are required during the manufacturing process. It should be noted that the large difference in the thermal expansion coefficient between these materials leads to the accumulation of deformation and high internal stress at the interface, which can ultimately lead to cracking [15]. Due to the aforementioned problems, the fabrication of bimetallic specimens with different interface designs between iron and copper alloys is challenging [16].

To manufacture a defect-free multi-component specimen when alternating dissimilar wires during printing, it is necessary to control the thermal conditions so that the wire of one material has time to melt, while the wire of the other material does not spread, creating defects and disrupting the geometry of the product. For this, it is necessary to take into account the physical and mechanical properties and calculate the values of heat input for each type of structural design and each material used, as will be shown below.

When forming a sharp interface between dissimilar materials, it is necessary to stop the deposition of one material before initiating the deposition of the other. Thus, immediately after depositing the N^{th} layer with iron alloy wire, the wire feed is switched to copper alloy wire (Fig. 3)

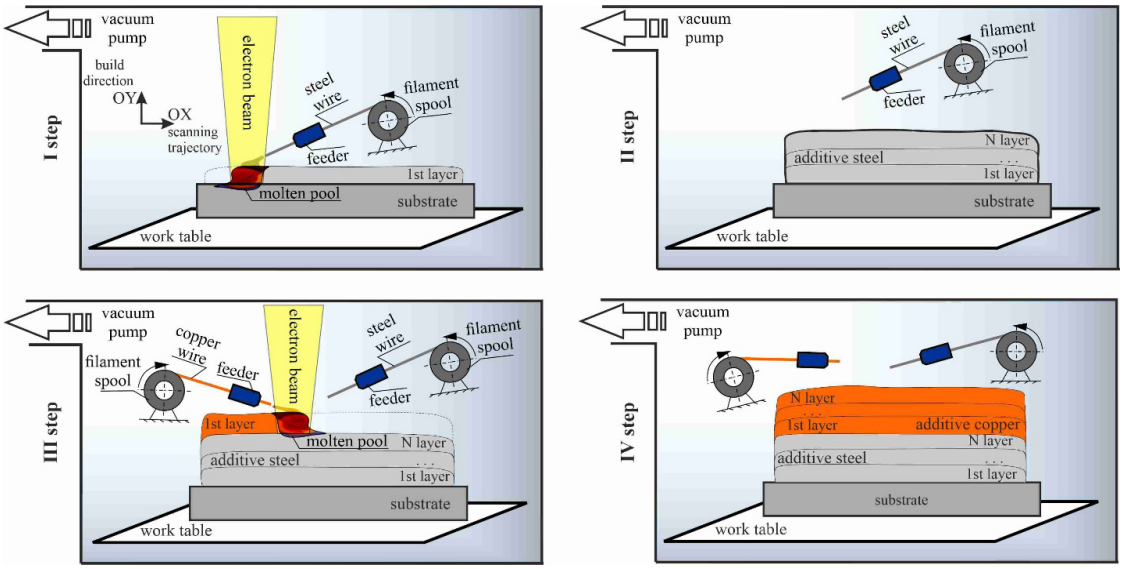

Fig. 3. Schematic of the wire-feed electron beam additive manufacturing process for fabricating bimetallic samples with a sharp interface between iron and copper alloys

To manufacture a bimetal with a sharp interface between iron and copper alloys, iron alloy wire was deposited layer by layer to create from 10 to 30 layers. Upon completion of the additively grown area of the iron alloy, the steel wire feed was completely stopped, and copper alloy wire was fed into the melt pool using a second feeder. Further, the $N + 1$ layers or the first layers of the copper alloy were deposited with different 3D printing parameters, taking into account the different physical and mechanical properties of the materials.

Visualization of changes in 3D printing parameters was carried out by changing the heat input values for each layer to gain a comprehensive understanding of the structures and defects in additively grown areas during manufacturing by additive methods. The heat input value is a characteristic of the thermal gradient, the amount of linear energy released per unit length of the layer [17]. The value of heat input in the manufacture of bimetallic specimens with a sharp interface between dissimilar materials is shown in Fig. 4.

The deposition of layers with iron alloy wire was carried out based on already known data [18]. Deposition of copper alloy wire layers using the same parameters is impossible. When selecting parameters

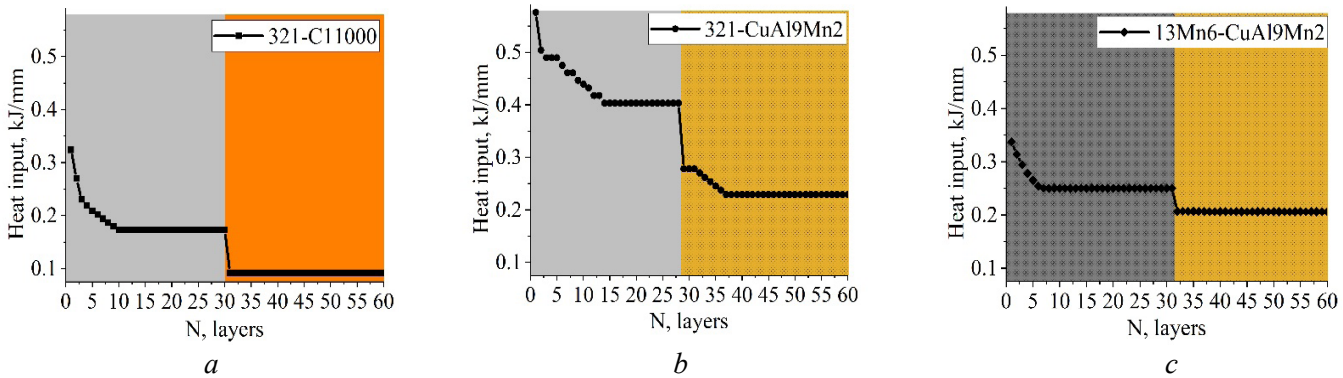

Fig. 4. Variation of heat input values as a function of layer during *EBAM* of a bimetallic sample with a sharp interface between dissimilar materials:

a – 0.12 C-18 Cr-9 Ni-Ti and *M1*; *b – 0.12 C-18 Cr-9 Ni-Ti* and *Cu-9 Al-2 Mn*; *c – 0.09 C-2 Mn-Si* and *Cu-9 Al-2 Mn*

for printing with copper wire on already deposited steel layers, it is necessary to minimize heat input. Thus, for printing bimetallic specimens based on iron and copper alloys, a fixed heat input value is set for each of the materials under consideration. The heat input value when depositing layers of copper *M1* is 0.09 kJ/mm, which is 2.5 times less than the heat input value when depositing layers of copper alloy *Cu-9 Al-2 Mn*. The heat input value when depositing layers of iron alloy 321 is 0.17 kJ/mm, which is 1.5 times less than the heat input value when depositing layers of iron alloy *0.09 C-2 Mn-Si*. This difference is due to the variation in thermophysical properties of the materials used. It should be noted that when applying the first layers to the substrate for each bimetallic specimen with a sharp interface, the heat input values are higher than the fixed ones. At such values, intensive heating of the substrate material occurs in the first layers of the specimen, which contributes to the stable formation of the melt pool. A common feature of the change in heat input values along the height of the printed specimen with a sharp interface is a sharp decrease during the transition from deposition of iron alloy to deposition of copper alloy.

When forming a smooth interface between dissimilar materials, iron and copper wires were fed simultaneously. It was necessary to gradually change the ratio of feed rates of iron and copper wires into the melt pool: the feed rate of the copper alloy wire into the melt pool needed to be increased simultaneously with decreasing the feed rate of the iron alloy wire until it completely stopped (Fig. 5). During the printing process, in the zone with a gradual change in the feed rate of wires of dissimilar materials, a structure with a smooth interface is formed.

During the feeding of only iron alloy wire when the copper alloy feed rate is $\upsilon_{copper} = 0$, a part of the additively grown steel is formed. The beginning of the smooth interface formation is accompanied by the introduction of copper alloy wire by the second feeder with a ratio of feed rates of the materials $\upsilon_{steel} > \upsilon_{copper}$ approximately 1 to 4. At this stage, the area with additively grown steel predominates until the ratio of feed rates of the materials becomes equal $\upsilon_{steel} = \upsilon_{copper}$. The formation of the smooth interface is completed when the volume of iron alloy wire introduced is reduced, when the ratio of feed rates of the materials is $\upsilon_{steel} < \upsilon_{copper}$ approximately 3 to 4. In the **IV** stage, only copper alloy wire is fed at iron alloy feed rate $\upsilon_{steel} = 0$, forming a part of additively grown copper. Thus, when manufacturing a vertical wall with a gradual change in feed rate, the formation of a smooth interface can be observed.

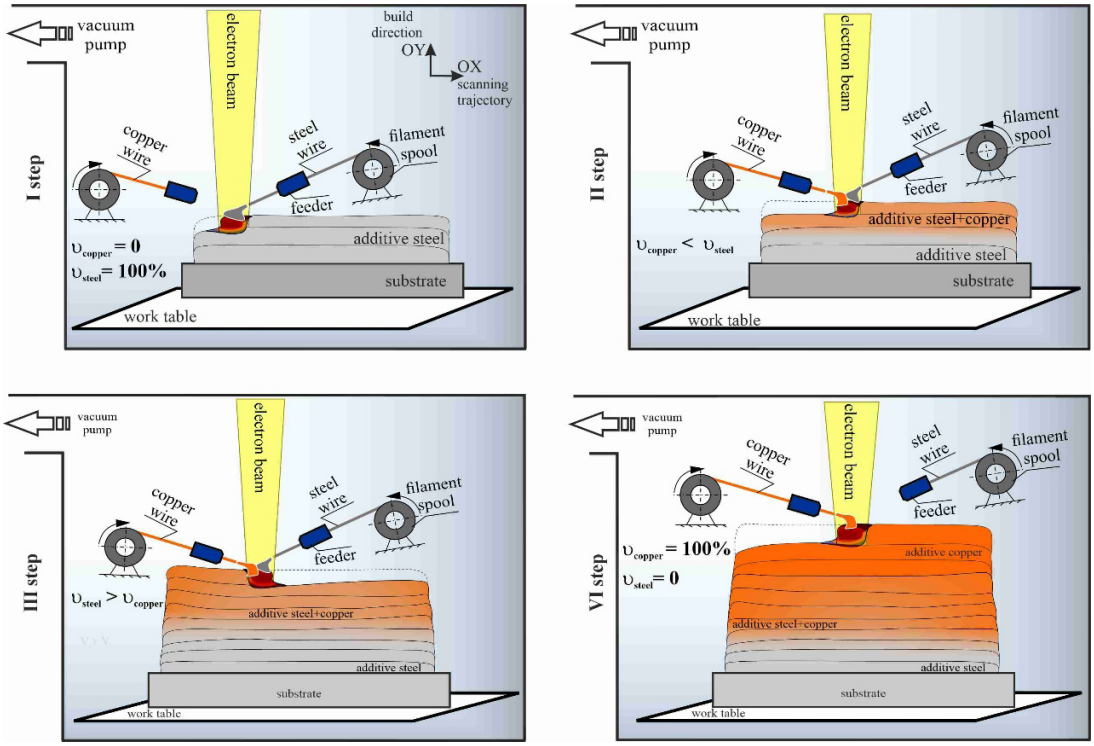

Fig. 5. Schematic of the wire-feed electron beam additive manufacturing process for fabricating bimetallic specimens with a smooth interface between iron and copper alloys

Similarly, to the gradual change in the feed rate of materials, the value of heat input also gradually changed along the height of the specimen (Fig. 6), unlike the change in heat input values depending on the layer when manufacturing bimetallic specimens with a sharp interface (Fig. 4). The heat input value when depositing layers of copper *M1* does not exceed 0.27 kJ/mm. The heat input value when depositing layers of stainless steel *AISI 321* is similar for both the manufacturing of bimetallic specimens with a smooth boundary of the *AISI 321 –M1* system and the *AISI 321-Cu-9 Al-2 Mn* system: in the first case, the value varies within 0.36- 0.23 kJ/mm, in the second case it varies within 0.38-0.28 kJ/mm, which is 1.5 times less than the heat input value when depositing steel layers during the manufacture of a bimetallic specimen of the *AISI 321 - Cu-9 Al-2 Mn* system. The heat input value when depositing layers of copper alloy *Cu-9 Al-2 Mn* during the manufacture of a bimetallic specimen of the *AISI 321 - Cu-9 Al-2 Mn* system does not exceed 0.23 kJ/mm, which is less than the heat input value for the *0.09 C-2 Mn-Si-Cu-9 Al-2 Mn* system. The heat input value during the manufacture of a bimetallic specimen of the *AISI 321-Cu-9 Al-2 Mn* system does not exceed 0.37 kJ/mm.

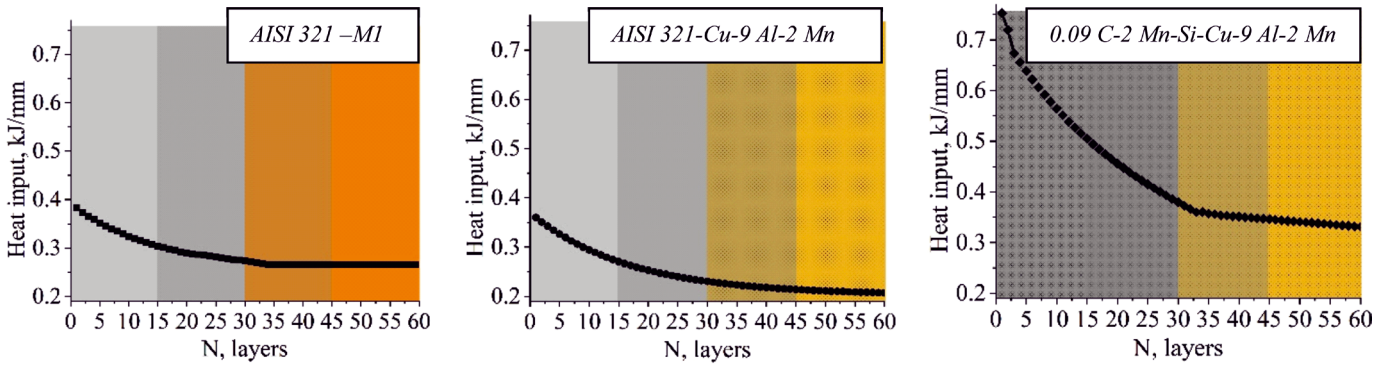

Fig. 6. Variation of heat input values as a function of layer during *EBAM* of a bimetallic sample with a smooth interface between dissimilar materials:

a – 0.12 C-18 Cr-9 Ni-Ti and *M1*; *b – 0.12 C-18 Cr-9 Ni-Ti* and *Cu-9 Al-2 Mn*; *c – 0.09 C-2 Mn-Si* and *Cu-9 Al-2 Mn*

When forming a heterogeneous structure in a bimetallic specimen, the printing strategy was changed depending on the percentage ratio of the volume of dissimilar alloy wires fed. In the case of a larger volume of copper wire fed in relation to the iron wire fed, only the first material was continuously fed while the second material was fed in droplets, discretely. Discrete wire feeding involves portioned delivery of material to the melting zone. This method allows precise control of the volume of material fed and reduces thermal overloads, which is especially important when working with materials sensitive to thermal deformations. However, this approach requires high precision synchronization between the movement of the electron beam and wire feeding, which complicates process control. From the perspective of electron scattering theory, discrete wire feeding is characterized by local exposure of the electron beam to the material. Nevertheless, there is a risk of uneven heat distribution, which can cause defects such as local overheating or insufficient melting. To minimize these effects, it is necessary to carefully calculate electron beam parameters, such as energy, focusing, and pulse duration, taking into account the properties of the material. In the case of equal or smaller volume of copper wire fed in relation to the iron wire fed, simultaneous continuous feeding of wires into the melt pool was performed – continuous printing strategy (Fig. 7). Continuous wire feeding provides constant delivery of material to the melting zone, which contributes to more uniform heat distribution and reduces the risk of defects such as pores or cracks. However, continuous feeding requires precise control of wire feed rate and electron beam power to avoid overheating or insufficient melting.

The difference in printing strategy is based on the strong differences in melting temperature and thermal conductivity of the materials used. When manufacturing bimetallic specimens with a smooth interface, it was found that the amount of material fed into the melt pool directly depends on the wire feed rate. To form

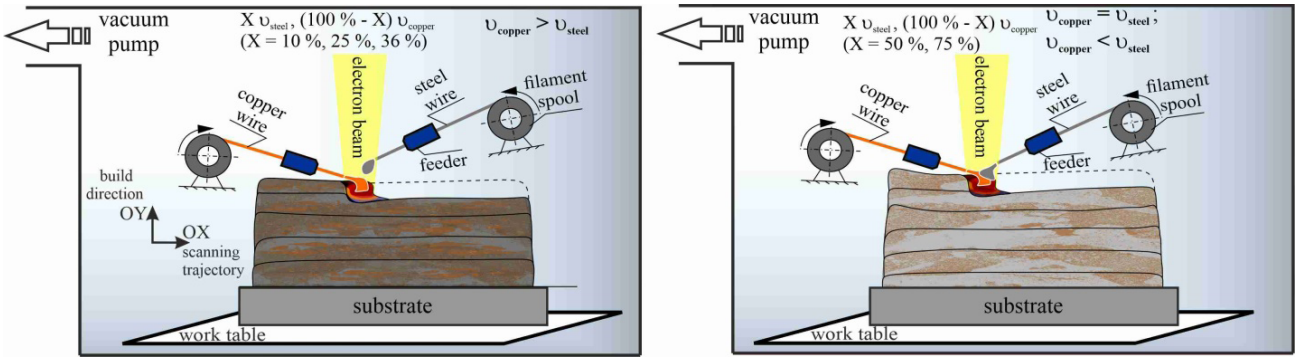

a *b*

Fig. 7. Schematic of the electron-beam additive manufacturing process for fabricating bimetallic samples with a heterogeneous structure using discrete (*a*) and continuous (*b*) printing strategies

a heterogeneous structure throughout the height, not just in the interface area, of a bimetallic specimen, it is impossible to create conditions for uniform melting for both copper alloy wires and copper alloy wires. Continuous deposition of both wires at a high feed rate of iron alloy wire leads to spreading of the copper alloy, disrupting the geometry of the bimetallic specimen with steel contents of 10 and 25 % in the copper matrix. Continuous deposition of both wires at a low rate leads to insufficient melting of the iron alloy wire in the melt pool. Droplet deposition at a high feed rate of iron alloy wire leads to spreading, which prevents the formation of the necessary specimen geometry. Therefore, for bimetallic specimens with a heterogeneous structure with a lower content of iron alloy, a discrete printing strategy was applied, and for specimens with a higher content of iron alloy, a continuous printing strategy was used.

In addition to controlling the type of wire feeding, printing strategy, and varying material feed rates, in the case of simultaneous feeding of dissimilar materials, special attention must be paid to changes in heat input values (Figs. 8-10).

The heat input value during the manufacturing of *AISI 321 –M1* composites with steel contents of 10 wt. % and 50 wt. % decreases from 0.38 to 0.26 kJ/mm, for *AISI 321 –M1*composites with steel content of 25 wt. %, the minimum value is 0.32 kJ/mm. A similar decrease in heat input values is also observed during the manufacturing of *AISI 321-Cu-9 Al-2 Mn* composites: when adding 10 wt. % and 25 wt. % of stainless steel *AISI 321*, the values decrease from 0.33 to 0.21 kJ/mm, when adding 25 wt. % the values decrease from 0.36 to 0.19 kJ/mm. A stable decrease in heat input values occurs in composites of the *0.09 C-2 Mn-Si-Cu-9 Al-2 Mn* system for each introduction of *0.09 C-2 Mn-Si* steel the values decrease from 0.33 to 0.19 kJ/mm.

For the manufacturing of composites, a common feature of changes in heat input values is a gradual decline. For composites of the *AISI 321 –M1* system with steel contents of 10 wt. %, 25 wt. %, and 50 wt. %,

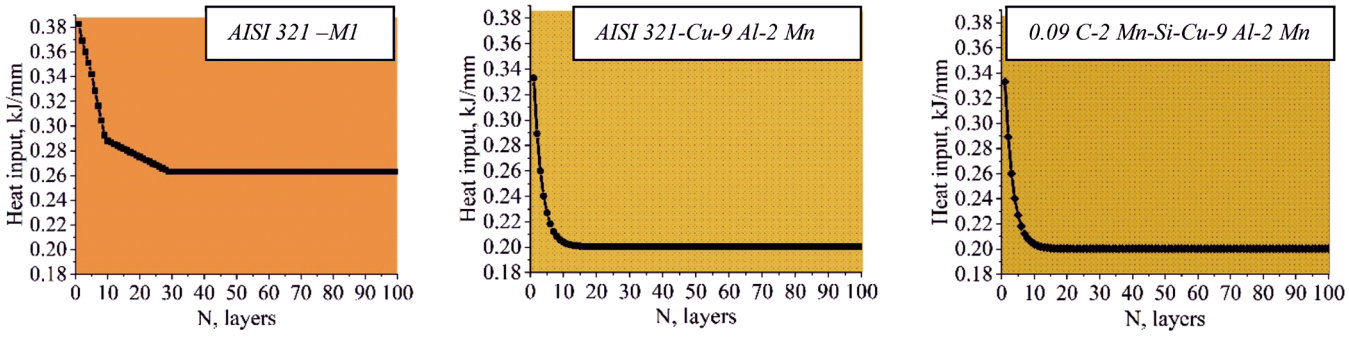

a *b* *c*

Fig. 8. Variation of heat input values as a function of layer during *EBAM* of a bimetallic samples with a heterogeneous structure containing 10 wt.% steel in a copper matrix:

a – 0.12 C-18 Cr-9 Ni-Ti and *M1*; *b – 0.12 C-18 Cr-9 Ni-Ti* and *Cu-9 Al-2 Mn*; *c – 0.09 C-2 Mn-Si* and *Cu-9 Al-2 Mn*

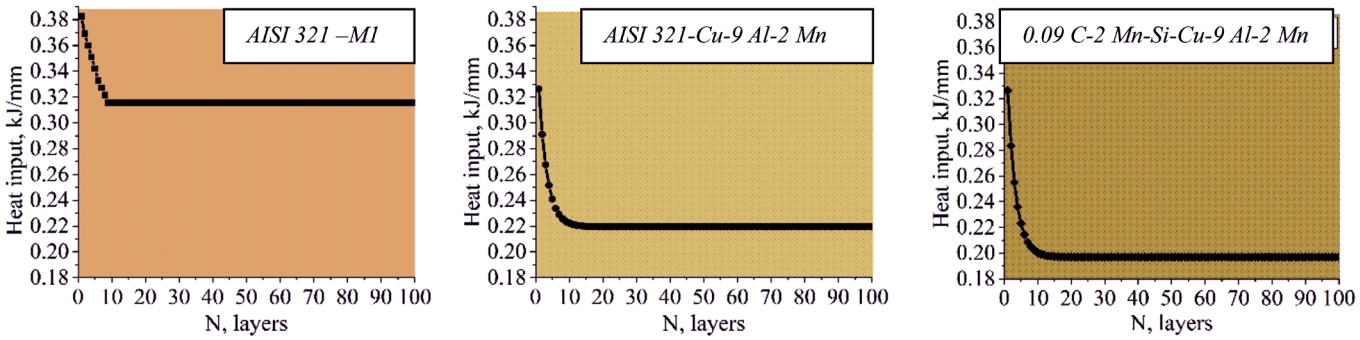

a *b* *c*

Fig. 9. Variation of heat input values as a function of layer during *EBAM* of a bimetallic samples with a heterogeneous structure containing 25 wt.% steel in a copper matrix:

a – 0.12 C-18 Cr-9 Ni-Ti and *M1*; *b – 0.12 C-18 Cr-9 Ni-Ti* and *Cu-9 Al-2 Mn*; *c – 0.09 C-2 Mn-Si* and *Cu-9 Al-2 Mn*

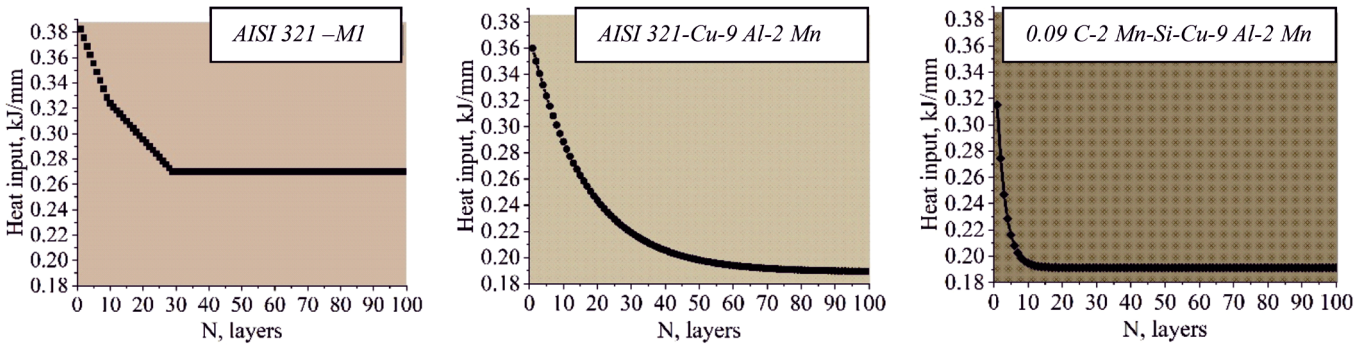

a *b* *c*

Fig. 10. Variation of heat input values as a function of layer during *EBAM* of a bimetallic samples with a heterogeneous structure containing 50 wt.% steel in a copper matrix:

a – 0.12 C-18 Cr-9 Ni-Ti and *M1*; *b – 0.12 C-18 Cr-9 Ni-Ti* and *Cu-9 Al-2 Mn*; *c – 0.09 C-2 Mn-Si* and *Cu-9 Al-2 Mn*

a linear decline in heat input values is observed from the first layer until the completion of manufacturing. For composites of the *AISI 321-Cu-9 Al-2 Mn* system with steel contents of 10 wt. %, 25 wt. %, and 50 wt. %, an exponential decline in heat input values is observed with different rates of decrease from the first layer until the completion of manufacturing. For *0.09 C-2 Mn-Si-Cu-9 Al-2 Mn* composites with steel contents of 10 wt. %, 25 wt. %, and 50 wt. %, an exponential decline in heat input values is observed with almost the same rate of decrease from the first layer until the completion of manufacturing.

Low heat input values when depositing steel wire are insufficient for complete melting of the filament and lead to areas with unmelted steel wire (Fig. 11, *a*).

High heat input values (from 500 kJ/m) allow complete melting of the iron alloy wire in the melt pool, preventing its overmelting. However, such heat input values increase the penetration depth of the electron

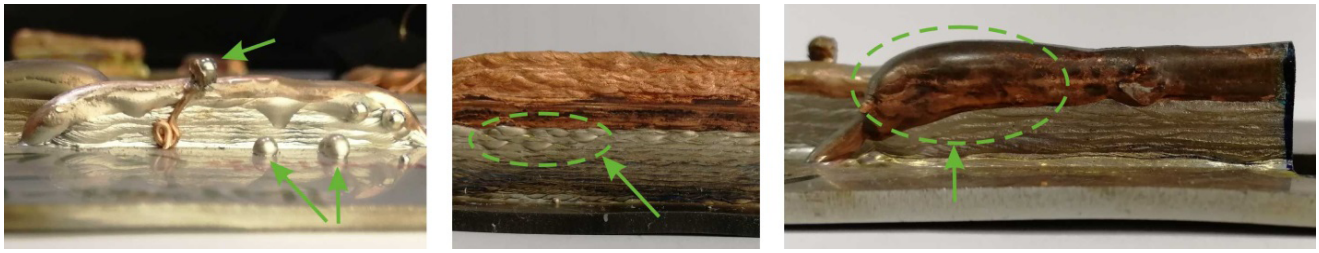

a *b* *c*

Fig. 11. Images of defects (complete melting (*a*), increased thickness (*b*) and wire non-melting (*c*)) during steel wire deposition, resulting from improperly selected parameters for bimetal fabrication using *EBAM*

beam, which leads to excessive melting of previously formed layers (Fig. 11, *b*). In the case of forming only the first layers of the manufactured product, they lead to bending of the substrate (Fig. 11, *c*). When applying a layer, material expansion occurs, which is limited by the colder deposited solidified layer, causing elastic compressive deformation. This leads to shrinkage of the material, causing a bending angle, and accumulates tensile residual internal stress in the growing direction.

Heat input values selected for steel wire deposition are high for copper wire deposition. This leads to complete melting of the fed material and its subsequent spreading on already deposited layers (Fig. 12, *a*). This increases the thickness of the product, which is an undesirable phenomenon (Fig. 12, *b*). Low heat input values are also undesirable for the formation of a defect-free product. This manifests in needle-like whole remnants of wire on the vertical wall (Fig. 12, *c*).

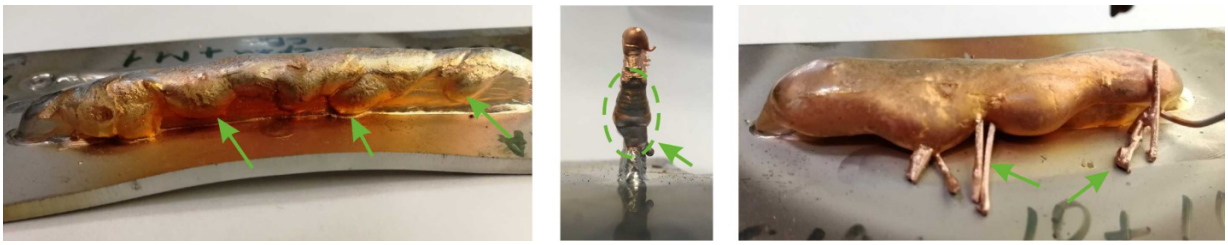

a *b* *c*

Fig. 12. Images of defects (complete melting (*a*), increased thickness (*b*) and wire non-melting (*c*)) during copper wire deposition, resulting from improperly selected parameters for bimetal fabrication using *EBAM*

When printing with set fixed parameter values for a bimetallic specimen with a smooth interface, it is necessary to control the heat input values from the very beginning until the last layer of the manufactured product. Controlling heat input values at each layer will help avoid the occurrence of discontinuities and delamination at the layer boundaries, which can lead to crack formation [19, 20]. In addition, insufficient or excessive energy input into the melt pool will lead to clumping of the fed material, which causes poor surface quality and disruption of the product geometry (Fig. 13). When applying the first layers to the substrate for manufacturing bimetallic specimens with any interface design, it is necessary to use a high heat input value. As the layer increases, it is necessary to reduce the heat input value. With this approach, sufficient heating of the material and a stable melt pool will occur.

Thus, based on the properties of the materials used, changing technological parameters is necessary for the manufacturing of defect-free metal products by additive manufacturing methods (Figs. 14-15).

Conclusions

1. Defect-free specimens of composite materials consisting of copper alloy and iron alloy were fabricated by the wire electron beam additive manufacturing method. To obtain heterogeneous materials, simultaneous and continuous metal feeding was performed into the 3D printing zone from two wire feeders.

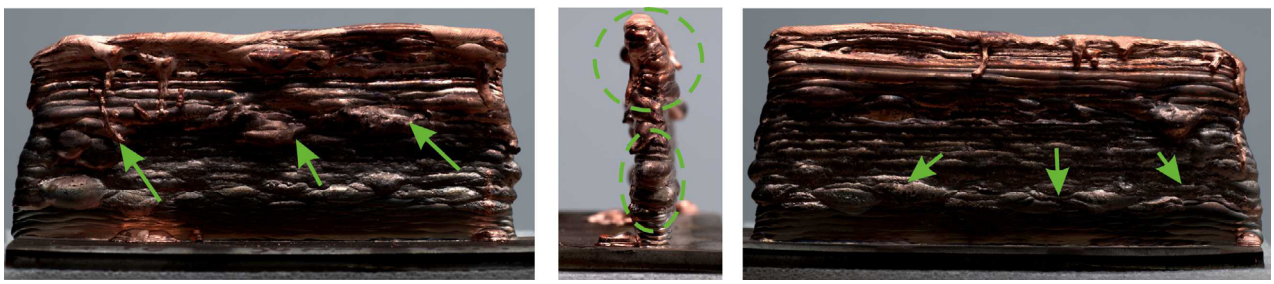

Fig. 13. Defects observed during copper wire deposition in *EBAM* bimetal fabrication due to improperly selected parameters

a *b*

Fig. 14. Defect-free bimetallic specimens fabricated by *EBAM* with optimal parameters:

a – sharp interface; *b* – smooth interface

a *b* *c*

Fig. 15. Defect-free steel-copper composites:

a – 10 % steel; *b* – 25 % steel; *c* –50 % steel

2. It has been established that the transition rate between dissimilar materials is reflected in the rate of change of heat input values as a function of layer number. To obtain a sharp interface between iron and copper alloys, a rapid reduction in heat input values is required, from 0.38 kJ/mm to 0.20 kJ/mm. When forming a smooth interface, a gradual decrease in heat input is necessary.

3. During the additive manufacturing of heterogeneous composites with simultaneous feeding of dissimilar materials, a complex process of component mixing in the liquid state and subsequent solidification occurs.

4. With a close ratio of volume fractions in heterogeneous samples of a composite specimen of the copper alloy and iron alloy system, it is necessary to use a continuous type of feeding. Conversely, when there is a significant difference in the volume fractions, a discrete feeding strategy is necessary.

References

1. Mehrpouya M., Tuma D., Vaneker T., Afrasiabi M., Bambach M., Gibson I. Multimaterial powder bed fusion techniques. *Rapid Prototyping Journal*, 2022, vol. 28 (11), pp. 1–19. DOI: 10.1108/RPJ-01-2022-0014.

2. Zadpoor A.A. Additively manufactured metallic porous biomaterials. *Journal of Materials Chemistry B*, 2019, vol. 7 (26), pp. 4088–4117. DOI: 10.1039/C9TB00420C.

3. Chen S., Huang J., Xia J., Zhao X., Lin S. Influence of processing parameters on the characteristics of stainless steel/copper laser welding. *Journal of Materials Processing Technology*, 2015, vol. 222, pp. 43–51. DOI: 10.1016/j.jmatprotec.2015.03.003.

4. Kučerová L., Zetková I., Jeníček Š., Burdová K. Hybrid parts produced by deposition of 18Ni300 maraging steel via selective laser melting on forged and heat treated advanced high strength steel. *Additive Manufacturing*, 2020, vol. 32, p. 101108. DOI: 10.1016/j.addma.2020.101108.

5. Raghuraman V., Widom M., Eisenbach M., Wang Y. First-principles residual resistivity using a locally self-consistent multiple scattering method. *Physical Review B*, 2024, vol. 109, p. 104204. DOI: 10.1103/PhysRevB.109.104204.

6. Wittenburg K. Specific instrumentation and diagnostics for high-intensity hadron beams. *CERN Yellow Reports*. Geneva, 2013, pp. 251–308. DOI: 10.5170/CERN-2013-001.251.

7. Gu D.D., Meiners W., Wissenbach K., Poprawe R. Laser additive manufacturing of metallic components: materials, processes and mechanisms. *International Materials Reviews*, 2012, vol. 57 (3), pp. 133–164. DOI: 10.1179/1743280411Y.0000000014.

8. Griffith M.L., Schlienger M.E., Harwell L.D., Oliver M.S., Baldwin M.D., Ensz M.T., Essien M., Brooks J., Robino C.V., Smugeresky J.E., Hofmeister W.H., Wert M.J., Nelson D.V. Understanding thermal behavior in the LENS process. *Materials & Design*, 1999, vol. 20 (2–3), pp. 107–113. DOI: 10.1016/S0261-3069(99)00016-3.

9. Angehrn N., Pagonakis I.G. A novel electron gun design approach with an externally assembled anode. *IEEE Transactions on Electron Devices*, 2023, vol. 70 (11), pp. 5934–5939. DOI: 10.1109/TED.2023.3317367.

10. Moritz J., Teschke M., Marquardt A., Stepien L., López E., Brückner F., Macias Barrientos M., Walther F., Leyens C. Electron beam powder bed fusion of γ-titanium aluminide: effect of processing parameters on part density, surface characteristics, and aluminum content. *Metals*, 2021, vol. 11 (7), p. 1093. DOI: 10.3390/met11071093.

11. Braun D., Ganor Y.I., Samuha S., Guttmann G.M., Chonin M., Frage N., Hayun S., Tiferet E. A design of experiment approach for development of electron beam powder bed fusion process parameters and improvement of Ti-6Al-4V as-built properties. *Journal of Manufacturing and Materials Processing*, 2022, vol. 6 (4), p. 90. DOI: 10.3390/jmmp6040090.

12. Hofmann D.C., Kolodziejska J., Roberts S., Otis R., Dillon R.P., Suh J.-O., Liu Z.-K., Borgonia J.-P. Compositionally graded metals: a new frontier of additive manufacturing. *Journal of Materials Research*, 2014, vol. 29, pp. 1899–1910. DOI: 10.1557/jmr.2014.208.

13. Kolubaev E.A., Rubtsov V.E., Chumaevsky A.V., Astafurova E.G. Micro-, meso- and macrostructural design of bulk metallic and polymetallic materials by wire-feed electron-beam additive manufacturing. *Physical Mesomechanics*, 2022, vol. 25, pp. 479–491. DOI: 10.1134/S1029959922060017.

14. Tang Y.T., Panwisawas C., Ghoussoub J.N., Gong Y., Clark J.W.G., Németh A.A.N., McCartney D.G., Reed R.C. Alloys-by-design: application to new superalloys for additive manufacturing. *Acta Materialia*, 2020, vol. 202, pp. 417–436. DOI: 10.1016/j.actamat.2020.09.023.

15. Osipovich K., Gurianov D., Vorontsov A., Knyazhev E., Panfilov A., Chumaevskii A., Savchenko N., Nikonov S., Rubtsov V., Kolubaev E. Phase formation, microstructure, and mechanical properties of Ni-Cu bimetallic materials produced by electron beam additive manufacturing. *Metals*, 2022, vol. 12, p. 1931. DOI: 10.3390/met12111931.

16. Tan C., Zhou K., Ma W., Min L. Interfacial characteristic and mechanical performance of maraging steel-copper functional bimetal produced by selective laser melting based hybrid manufacture. *Materials & Design*, 2018, vol. 155, pp. 77–85. DOI: 10.1016/j.matdes.2018.05.064.

17. DebRoy T., Wei H.L., Zuback J.S., Mukherjee T., Elmer J.W., Milewski J.O., Beese A.M., Wilson-Heid A., De A., Zhang W. Additive manufacturing of metallic components – Process, structure and properties. *Progress in Materials Science*, 2018, vol. 92, pp. 112–224. DOI: 10.1016/j.pmatsci.2017.10.001.

18. Tarasov S.Yu., Filippov A.V., Savchenko N.L., Fortuna S.V., Rubtsov V.E., Kolubaev E.A., Psakhie S.G. Effect of heat input on phase content, crystalline lattice parameter, and residual strain in wire-feed electron beam additive manufactured 304 stainless steel. *The International Journal of Advanced Manufacturing Technology*, 2018, vol. 99, pp. 2353–2363. DOI: 10.1007/s00170-018-2643-0.

19. Wu S., Yang Y., Huang Y., Han C., Chen J., Xiao Y., Li Y., Wang D. Study on powder particle behavior in powder spreading with discrete element method and its critical implications for binder jetting additive manufacturing processes. *Virtual and Physical Prototyping*, 2023, vol. 18 (1), pp. 1–26. DOI: 10.1080/17452759.2022.2158877.

20. Bourell D., Kruth J.P., Leu M., Levy G., Rosen D., Beese A.M., Clare A. Materials for additive manufacturing. *CIRP Annals Manufacturing Technology*, 2017, vol. 66, pp. 659–681. DOI: 10.1016/j.cirp.2017.05.009.

Conflicts of Interest

The authors declare no conflict of interest.